

## COMPARISONS OF AN EVOLUTIONARY CHEMICAL MODEL WITH OTHER MODELS

JEONG-EUN LEE

*Department of Astronomy, The University of Texas at Austin, 1 University Station C1400, Austin, Texas 78712-0259*

NEAL J. EVANS II

*Department of Astronomy, The University of Texas at Austin, 1 University Station C1400, Austin, Texas 78712-0259*

AND

EDWIN A. BERGIN

*Department of Astronomy, The University of Michigan, 825 Dennison Building Ann Arbor, Michigan 48109-1090*

*Draft version December 23, 2018*

### ABSTRACT

We compare an evolutionary chemical model with simple empirical models of the abundance and with static chemical models. We focus on the prediction of molecular line profiles that are commonly observed in low mass star forming cores. We show that empirical models can be used to constrain evaporation radii and infall radii using lines of some species. Species with more complex abundance profiles are not well represented by the empirical models. Static chemical models produce abundance profiles different from those obtained from an evolutionary calculation because static models do not account for the flow of matter inward from the outer regions. The resulting profiles of lines used to probe infall may differ substantially.

*Subject headings:* ISM: astrochemistry – ISM: molecules – stars: formation

### 1. INTRODUCTION

Most theoretical studies of the process of star formation for low mass stars (Larson 1969; Penston 1969; Shu 1977; Terebey, Shu, & Cassen 1984; Shu, Adams, & Lizano 1987; Foster & Chevalier 1993; Ciolek & Mouschovias 1994; McLaughlin & Pudritz 1997) focus on the formation of single stars, because these stars are simple test sites with less observational confusion. Such theories provide different predictions about density and velocity structures as a function of time. In principle, observations in dust continuum emission and molecular transitions can be converted to these same physical quantities to test theory. However, in practice the conversion is not trivial, and one should use detailed models in a self-consistent way to correctly assess physical conditions in star forming cores. The density and temperature profiles of a core can be determined from comparison of the dust continuum observations with a continuum radiative transfer calculation. However, the velocity structure, which is the key to the dynamics of the entire star formation process, is not easily inferred directly from the observations of molecular transitions because it is coupled with abundance profiles, which vary along the line of sight due to the interactions between gas and dust grains (freeze-out and desorption of molecules on and off grain surfaces). Therefore, the dynamics is entangled with the chemistry.

In order to test various theoretical infall models, an evolutionary sequence of line profiles should be generated self-consistently to compare with a wide range of observations. Lee et al. (2004, hereafter Paper I) established a self-consistent model, where a dynamical model (the inside-out collapse model preceded by evolution through

a sequence of the Bonnor-Ebert spheres) was coupled with chemistry and thermal balance in order to simulate the evolution of molecular line profiles. The model has been tested by comparison with observations (Young et al. 2004; Evans et al. 2005). Alternatively, simple empirical models of step or drop functional abundance structures (Schöier et al. 2002; Lee et al. 2003; Jørgensen et al. 2004) have been used to fit observations. However, according to Paper I, the abundance structures of some molecules are very complicated, so they are not reasonably approximated with a simple function. Static models (Doty et al. 2002; Doty et al. 2004), which involve the actual calculation of the chemical evolution but adopt constant physical conditions with time, have been used to compare the abundance profiles across the envelopes with observational data and empirical profiles. In the prestellar stage, the static model could work because the dynamical timescale is long enough compared to the chemical timescale. However, after collapse begins, the timescales for depletion and gas-phase chemistry are comparable to the dynamical timescale (see Table 4 in Paper I). In addition, the evaporation of molecules modifies the gas-phase chemistry dramatically. While evaporation was included in static models, they did not include the effect of fresh material being brought into the evaporation zone. As a result, the static models might give misleading abundance profiles.

In this paper we compare the evolutionary model established in Paper I with empirical models such as drop and step functions that have been used in the literature (Lee et al. 2003; Jørgensen et al. 2004; Young et al. 2004; Evans et al. 2005). Then we compare the evolutionary model with a static chemical model. Our aim is two-fold: first, to explore what can be learned from the more easily applied simple, empirical models; and second, to learn the differences between the predictions of

evolutionary models and the simpler, static models.

## 2. COMPARISON WITH EMPIRICAL MODELS

### 2.1. Method

In this section, we take the results of the evolutionary model as representative of the true situation and produce line profiles from them. The line profiles are calculated for typical observing parameters and a cloud distance of 140 pc, the distance to typical nearby regions of star formation. Then we try to match these line profiles by adjusting the free parameters in empirical models to get the best match to the line profiles from the evolutionary calculation. Then we ask how well certain parameters, such as the evaporation radius ( $R_{evap}$ ; §2.2), infall radius ( $r_{inf}$ ; §2.3) and outer radius ( $r_{out}$ ; §2.3) are determined by the fit of the empirical models. The fit is evaluated by using the absolute deviation (AD). Two kinds of AD values are computed. For a given line, the AD is computed from  $\sum_i |T_R(evap; i) - T_R(emp; i)|/N$  where  $N$  is the number of points in the line profile. For a species, the AD is computed from the integrated intensities over the transitions modeled ( $AD = \sum_j |I(evap; j) - I(emp; j)|/n$  where  $j$  indicates different transitions, and  $n$  is the total number of transitions). In almost all cases, these two measures agreed on the best fit. We use the average of the two ADs to decide the best fit in the cases that they do not agree. C<sup>18</sup>O and CS lines are tested for this comparison since these molecular lines are the most frequently used to trace low mass star forming cores, and the collision rates for those molecules have been well studied.

The evolutionary model used for the comparison assumes that a sequence of the Bonnor-Ebert spheres represents the evolution of a dense core in the pre-protostellar stage, and the core evolves based on the inside-out collapse model in the protostellar stage. The time step of  $t = 0$  is considered as the end of the pre-protostellar stage and the initiation of collapse. For comparison to empirical models, we adopt abundance profiles at the time step of  $t = 10^5$  yr, when the infall radius is 0.0227 pc (about 33'' at 140 pc) with the sound speed of 0.22 km s<sup>-1</sup>. The chemical network in the model considers gas-grain interactions as well as the gas-phase chemistry, and it assumes bare SiO<sub>2</sub> grain surfaces and an external extinction of 0.5 mag (refer to Paper I for details). The binding energy of CO onto the SiO<sub>2</sub> grain surfaces is assumed to be 1181 K (see Table 2 of Paper I).

Of course, other physical, dynamical, and chemical models may describe the actual situation, but comparison to the model described here should provide some insights into the more general case.

### 2.2. Drop and Step Models

In prestellar cores, molecules are frozen-out onto grain surfaces in the inner regions, so the abundance profile can be approximated with a step function (Lee et al. 2003) with a low abundance at small radii and a high abundance at large radii (3 free parameters per species). This step function corresponds to the jump or anti-jump model in the notation of Jørgensen et al. (2004). However, once a central protostar forms, the inner regions are heated. As a result, molecules evaporate in these regions, so abundance profiles are assumed to become similar to a drop function. A drop function has three

zones to describe 1) the innermost zone with a high abundance caused by evaporation of a molecule, resulting from the heating by the newly formed protostar 2) an intermediate zone with low (drop) abundance caused by freeze-out of the molecule onto grain surfaces in regions with low temperatures and high densities, and 3) the outermost zone with high abundance at large radii (the same abundance as in the inner zone), where densities are low, so the freeze-out timescale is longer than the dynamical timescale. The drop function thus has 4 free parameters per species (the high abundance, the drop abundance, and the inner and outer radii of the drop section). Jørgensen et al. (2004, 2005) used drop functions to describe the evolution of abundance profiles in protostellar cores. In their description, the region of evaporation becomes larger, and the drop becomes narrower as the central protostar evolves.

Fig. 1 compares the CS 2–1 lines from the evolutionary model at the time steps of  $t = 0$  and  $t = 10^5$  yr with various resolutions. As described above and in Fig. 1a, CS is frozen-out at small radii at  $t = 0$  yr, but at  $t = 10^5$  yr, CS has high abundances at small radii due to heating by the central protostar and accretion on to the protostar. The evolutionary stages are more easily distinguished at higher resolution.

The question addressed in this section is the following: how well can the empirical models determine the evaporation radius ( $R_{evap}$ )? For this test, we adopt abundance profiles at the time step of  $t = 10^5$  yr from the evolutionary model as a standard for comparison. At this time, the CO evaporation radius in the model,  $R_{evap} = 0.003$  pc, corresponding to 4.4'' at 140 pc. We have then tuned drop models to fit line profiles simulated with the standard evolutionary model as well as possible. We did not explore a complete grid of models. Instead, we first chose the four parameters of the drop function based on the evolutionary model and tuned the parameters to find a reasonably good fit. This process simulates a procedure in which a model of continuum emission provides a dust temperature distribution and knowledge of evaporation temperatures is used to select the inner boundary of the drop region. Once the first good fit model was obtained, we varied each parameter by some factors to check that the fit was still the best, or to find a better fit.

The CO abundance profiles of the two models are plotted in Fig. 2a. In the figure, at large radii, the high abundance of the drop function is similar to the normal abundance of the evolutionary model. In addition, the best-fit inner boundary of the drop zone ( $R_{evap}$ ) is located almost at the same radius as the evaporation front in the standard evolutionary model. Fig. 2c compares the line profiles of three C<sup>18</sup>O transitions simulated with the abundance profiles in Fig. 2a with the resolutions that have been used in Jørgensen et al. (2002). The line profiles from the two models are almost identical. According to the tests of various drop functions, we found that the CO evaporation front, which is located at 0.003 pc, could be well constrained by the simple model (Fig. 2b). If we use evaporation radii smaller and larger than that (0.003 pc) of the best model by a factor of two, that is, 0.0015 and 0.006 pc, the absolute deviations calculated by comparisons between line profiles simulated from the standard model and drop models with the two

evaporation radii are greater than that of the best drop model by factors of about 5 and 7, respectively. The biggest variation of AD occurs in the 3–2 line because the higher C<sup>18</sup>O transition has the highest critical density, and the resolution for the 3–2 line is smallest, so the 3–2 line is the most sensitive to the size of the high abundance zone at small radii. As a result, the CO evaporation front, which determines the size of the high abundance zone in the regions with high densities, can be well constrained by drop models if the proper transition and adequate resolution are used.

The CS 2–1 lines with various resolutions are shown in Fig. 3. In this comparison, we have tested both step and drop functions, and Fig. 3a shows the drop and step abundance profiles that best match the evolutionary model at  $t = 10^5$  yr. The results from the drop and step models shown in Fig. 3a are compared to the result from the evolutionary model in Fig. 3b and 3c, respectively. Drop functions cause self-absorptions to be deeper than the evolutionary model because of high abundances at large radii. Step functions work better for the self-absorption dips in the CS 2–1 line in this comparison since the less attenuated ISRF reduces the CS abundance at large radii significantly. However, as seen in Fig. 4 (Fig. 13 of Paper I), the CS abundance structure resulting from the model with 3 mag of external extinction is more closely approximated with a drop function because it has higher abundance at the outer radii, caused by lower photodissociation by interstellar UV photons. If higher spatial resolution is used, neither a step function nor a drop function fits the high velocity wings (the third panels of Fig. 3b and 3c) that are produced by the high abundance at very small radii. Of course, the high velocity wings from infall may be confused by outflow in a real source.

There are two jumps of the CS abundance profile in the evolutionary model; one is associated with CO evaporation at 0.003 pc, and the other is caused by the evaporation of CS itself at 0.001 pc. In both functions, the CO evaporation front is well constrained by the CS line as it was in the CO line profiles. The better constraint is given by the higher resolution observation. The critical density of CS 2–1 is about  $2 \times 10^5$  cm<sup>−3</sup>, and the density around the CO evaporation radius at  $t = 10^5$  yr is not very different from the critical density, so the 2–1 line, even with lower resolution, is affected by the location of the CO evaporation front. The CS evaporation front cannot be constrained with this kind of simple step or drop function. The evaporation of CS from grain surfaces occurs at very small radii ( $r < 0.001$  pc) with high temperatures, so if the abundance jump of CS at the CO evaporation radius is ignored, the intensity and width of simulated lines are too small compared to the evolutionary model. Functions with two steps and observations with high resolution might be able to constrain the CS evaporation front as well as the CO evaporation front.

The difference between the evolutionary model and the empirical model is more significant in transitions from higher energy levels at high spatial resolutions. Fig. 5 shows the comparison of the CS 5–4 lines from the evolutionary and step function abundance profiles. The red peak and blue wing around  $\pm 1.5$  km s<sup>−1</sup> are caused by the abundance peak at  $R_{evap}(\text{CS})$  ( $\leq 0.001$  pc). The abundance peak also increases the peak radiation tem-

perature by a few K. Even though the volume of the inner small region where CS has its abundance peak is very small, high density and temperature combined with the abundance peak cause high excitation of CS.

### 2.3. Variations in the Physical Model

In this section, we address the question: how well can the empirical models determine the infall radius ( $r_{inf}$ ) and the outer radius ( $r_{out}$ )? For this test, we retain the same evolutionary model at  $t = 10^5$  yr, which produces an infall radius,  $r_{inf} = 0.0227$  pc, with an outer radius,  $r_{out} = 0.15$  pc, but we change the relevant radii in the empirical model by a factor of two in either direction to see if the fit to the observations degrades.

First we change the infall radius and simulate the CS 2–1 line. In this test, we assumed the same luminosity (about  $1 L_\odot$ ), which can be constrained by observations, and kinetic temperature structures were calculated self-consistently. The CS 2–1 line has been simulated with a resolution of 30''. In Fig. 6, profiles drawn with the dotted line show the best step models with different infall radii compared to the evolutionary model at  $t = 10^5$  yr. The physical models with different infall radii are illustrated in Fig. 7. In Fig. 7d, abundance profiles of the three best step models are compared with that of the evolutionary model. We tested different higher and lower abundances in step models, but all the best step models finally had the same higher ( $4.0 \times 10^{-9}$ ) and lower ( $4.0 \times 10^{-10}$ ) abundances. The inner region of the CS higher abundance is smaller in the model with the smaller infall radius, and vice versa. The higher and lower densities in the model with the smaller and larger infall radii produce stronger and weaker CS 2–1 lines, respectively, as shown in Fig. 6. The model with the smaller infall radius has smaller velocities (Fig. 7c) within the infall radius, so the simulated line profile is narrower than the CS 2–1 line profile from the evolutionary model (the first panel of Fig. 6). On the other hand, the model with the larger infall radius produces broader line profiles (the third panel of Fig. 6). These trends are also found in the higher transitions of CS, which can trace denser regions, simulated with the spatial resolutions that are currently available. Based on this test, we think that the infall radius of a core collapsing from the inside-out might be constrained by a simple model such as the step model with optimized abundances. This result is consistent with that of Evans et al. (2005), who found that evolutionary and step function models agreed on the  $r_{inf}$  needed to match observations of CS in B335.

The determination of the outer radius has been also tested with CS 2–1. We decreased and increased the outer radius by a factor of 2 in the step model. In our standard evolutionary model, the outer radius is 0.15 pc. The infall radius is the same (0.0227 pc) in all models, so the velocity structure is also the same in all models. The kinetic temperature structure for each model has been calculated self-consistently, and the abundance profile in three different models are the same step function as shown in Fig. 3a. Fig. 8 compares the line profiles simulated from models of different outer radii with the same luminosity, infall radius, and step abundance profile with the line profile from the evolutionary model at  $t = 10^5$  yr. The result does not show big differences in models with different outer radii. We also used C<sup>18</sup>O transitions,

which trace less dense regions better than CS transitions, for this test and found that  $\text{C}^{18}\text{O}$  might constrain only the minimum value of  $r_{out}$  with the  $1 - 0$  line. However, the higher transitions of  $\text{C}^{18}\text{O}$ , as with CS lines, did not show big differences in models with different outer radii. We tested the line ratios of CS and  $\text{C}^{18}\text{O}$  as a constraint of the outer radius. The line ratios of CS were similar for different outer radii, but the line ratios of  $\text{C}^{18}\text{O}$  showed the possibility of constraining the outer radius. If we use outer radii smaller and larger than 0.15 pc by a factor of two, that is, 0.075 and 0.30 pc, the ADs are greater than that of the model with  $r_{out} = 0.15$  pc by factors of 4.5 and 2.5, respectively. Therefore, in order to constrain the outer radius of an isolated core, one might have to observe multiple lines of appropriate molecules such as  $\text{C}^{18}\text{O}$  and calculate their line ratios. In the case of star forming cores associated with bigger molecular clouds, however,  $\text{C}^{18}\text{O}$  is not a good choice because the  $1 - 0$  line emission will be contributed partly by the extended molecular cloud, so even its line ratios will not constrain outer radii.

We also tested the step model to constrain the infall radius and outer radius with CS lines at a different time step,  $t = 3 \times 10^5$  yr. The infall radius at that time step is about 0.0703 pc. Using this test, we find the same result as before at  $t = 10^5$  yr, that the outer radius is not well constrained by the simple model of CS. However, we could constrain only the minimum infall radius with the step model of CS at  $t = 3 \times 10^5$ , unlike the result at  $t = 10^5$  yr. At later times, the infall radius is large, and the densities around the infall radius are too low to be traced well by the CS lines. Therefore, other molecular lines that have lower critical densities need to be used to constrain the infall radius in later evolutionary stages.

### 3. COMPARISON WITH STATIC MODELS

The next step beyond empirical models is a time dependent chemical model calculated for a static physical model. Doty et al. (2004) used density and temperature structures obtained by Schöier et al. (2002) in order to test the chemical distribution across the envelope of IRAS 16293-2422. Even though they calculated the chemical evolution, the physical (density and temperature) structures were not varied with time. As a result, the evaporation fronts of molecules, which affect molecular line profiles significantly, stay at the same radii with time. However, the density structure should change with time in any dynamical theory, and the temperature structure varies with time depending on the accretion rate and mass of the star (thus the evolution of luminosity). In Paper I, we have adopted Shu's picture as the standard for the dynamical evolution providing a constant accretion rate, so the central luminosity, thus the dust temperature, increases ( $L \propto M_*$ ). As a result of the evolution of the temperature structure, the evaporation fronts propagate outward with time. In this study, therefore, we compare the evolutionary model with two flavors of static models: a truly static model and a partly static model. The truly static model does not have the variation in physical conditions as in Doty et al. (2004). In the partly static model, we consider the evolution of physical conditions based on Shu's inside-out collapse model and the results of dust continuum radiative transfer calculations without following each gas parcel.

Fig. 9 shows the comparison between the evolutionary model and the truly static model. We adopt density and temperature structures from the evolutionary model at the time step of  $t = 10^5$  yr, as shown in Fig. 7a and 7b with the solid lines. For this comparison, we use the standard chemical model in Paper I, where the molecular binding energies onto the bare  $\text{SiO}_2$  grain surfaces are considered and the ISRF is attenuated by 0.5 mag. The same initial abundances, shown in Table 3 of Paper I, have been used in both the evolutionary model and the truly static model. The left and right panels of Fig. 9 compare the abundance profiles from the truly static model at  $t = 10^5$  and  $t = 1.1 \times 10^6$  yr, respectively, with those of the evolutionary model at the time step of  $t = 10^5$  yr. In the evolutionary model, the model core spent  $1 \times 10^6$  years in the pre-protostellar stage, so the whole timescale for the chemical evolution at  $t = 10^5$  yr is  $1.1 \times 10^6$  years.  $\text{CO}$ ,  $\text{CS}$ ,  $\text{H}_2\text{CO}$ , and  $\text{HCO}^+$  are molecules that reach their maximum abundances fast, so they are already in the phase of depletion at  $t = 10^5$  yr. However, nitrogen-bearing molecules such as  $\text{NH}_3$  and  $\text{N}_2\text{H}^+$  are related to  $\text{N}_2$ , which forms slowly, so those molecules become more abundant even until  $t = 1.1 \times 10^6$  yr. In the truly static model, the abundances of those nitrogen-bearing molecules never reach the maximum values within the  $\text{CO}$  evaporation radius because the abundant  $\text{CO}$  will destroy them directly or indirectly. The biggest difference between the evolutionary model and the truly static model in the right panel is shown in the  $\text{CS}$  abundance profiles; a deep depletion zone between  $R_{\text{evap}}(\text{CS})$  and  $R_{\text{evap}}(\text{CO})$  in the static model. This difference is due to the dynamical effect. In the evolutionary model, the material with a high  $\text{CS}$  abundance in the outer region around  $R_{\text{evap}}(\text{CO})$  continues to flow into the zone to cancel out the depletion effect, but in the static model, the depletion of  $\text{CS}$  occurs continuously from the same material to reduce the abundance more with time in that zone. The other difference is the occurrence of peaks inside the  $\text{CO}$  evaporation radius. For example, for  $\text{H}_2\text{CO}$  and  $\text{HCN}$ , the peaks that appear in the evolutionary model disappear in the truly static model because no fresh material is brought in to radii smaller than  $R_{\text{evap}}(\text{CO})$  to sustain the peaks in the static model, unlike in the evolutionary model.

In the partly static model, we simply assume that the physical conditions evolve without any dynamical process, as in Bonnor-Ebert spheres, and calculate the chemical evolution at given radii in an Eulerian coordinate. In contrast, in the evolutionary model of Paper I, the chemical evolution has been calculated in a Lagrangian coordinate system following all gas parcels as they fall toward the center and transferred to an Eulerian coordinate system to provide abundance structures at any time step. Even though we see the same physical conditions at a given radius at a given time step in the two models, the histories of physical conditions that a gas parcel in the two models goes through until the given time step are totally different. As illustrated in Fig. 10, in the inside-out collapse, the density evolves from lower to higher while the chemical evolution of a given gas parcel is calculated in the evolutionary model. On the contrary, in the partly static model, the chemical evolution is calculated at a given radius, so the density evolves from higher to lower. In addition, the evolution-

ary model always experiences a lower temperature than the partly static model does until the given time step after the central protostar forms, since the gas parcel in the evolutionary model is located at a radius greater than the radius where the partly static model is calculated at all times until the given time step. Thus, the past history of physical conditions affect the depletion and evaporation of molecules, causing differences in their abundance structures and, finally, line profiles.

For the comparison between the evolutionary model and the partly static model, as described above, we use the standard chemical model in Paper I. The partly static model spends  $10^6$  years in the pre-protostellar stage passing through a sequence of Bonnor-Ebert spheres before collapse, as does the evolutionary model. Therefore, the initial abundances for the chemical evolution after collapse are the same in the two models. Fig. 11 shows the differences of abundance profiles resulting from the evolutionary model and the partly static model at  $t = 10^5$  yr after collapse begins. First, outside the infall radius (about 0.023 pc), the two models show identical abundance profiles since no dynamical motion is involved. However, the partly static model shows more freeze-out of molecules between the infall radius and the CO evaporation front, due to the history of higher densities in the static model. In the evolutionary model, a gas parcel moves from an outer radius to the given radius carrying less frozen-out material. In the static model, the evaporation fronts are also located at slightly larger radii than in the evolutionary model because the static model always experiences higher temperatures than does the evolutionary model after the central protostar forms, and the time interval between two time steps is not infinitesimal in the evolutionary calculations. The biggest difference between two models lies in the abundance peaks caused by the evaporation of molecules other than CO. In the static model, the peaks are very weak or disappear. The difference is caused by the dynamical effect; that is, in the static model, once molecules evaporate and reach chemical equilibrium, no more evaporation occurs from grain surfaces. However, in the evolutionary model, material is being fed into these regions to sustain high abundance peaks. This material effectively produces an abundance pile-up at the evaporation front for a given volatile as the grains sweep past. The structures in the evolutionary model are also smeared in radius as a result of the dynamical effect. These differences will be more significant in other dynamical models with higher velocities. We also tested the case of water dominant grain surfaces, and the results show that the difference between the static model and the evolutionary model is more significant because more freeze-out is caused by higher binding energies.

Among molecules in Fig. 11, the most significant difference between the partly static model and the evolutionary model is seen in CN, so one can expect the greatest difference in CN line profiles too. However, we do not have good collision rates for the transitions of CN; we therefore focus on H<sub>2</sub>CO instead. In Fig. 12, we compare H<sub>2</sub>CO line profiles resulting from abundance profiles of the two models to show that the ratio between blue and red peaks, which increases as the infall speed increases, is smaller in the static model if a high resolution (3'') is used. In addition, as a result of the inner zone of the high H<sub>2</sub>CO abundance in the evolutionary model,

the line profile from the evolutionary model is broader than that from the static model. The peak intensities are also stronger by about a factor of 2 in the evolutionary model. Therefore, it is possible to infer faster infall velocities than the actual infall velocity by using the static model. In the simulation of line profiles, we adopt the velocity structure of the inside-out collapse at  $t = 10^5$  yr for both the evolutionary model and the static model even though the static model assumes no dynamical motion in the chemistry.

The difference between the partly static and evolutionary models occurs within the infall radius, which increases with time, so the difference can only be caught by molecular observations with very high resolutions, in the earlier evolutionary stages. Therefore, the velocity structure is entangled with abundance structures at small radii, which might be possibly connected to disk dynamics as well as envelope dynamics, but it will be constrained by telescopes such as CARMA and ALMA, which will become available in the near future.

#### 4. CONCLUSIONS

Although actual abundance profiles cannot be matched completely by the empirical models, our comparisons suggest the empirical models may fit line profiles of CO and its isotopes. CO has a relatively simple abundance profile and hence can be more readily matched. However, the empirical models are very different for other molecules (e.g., CS, H<sub>2</sub>CO, CN), which have more complicated abundance profiles in the inner zones (Paper I). For these more complicated models the disparity between the empirical model and the true profile is magnified with higher spatial resolution in higher energy level transitions. However, we can still learn about  $R_{evap}$  and  $r_{inf}$  from the empirical models applied to appropriate lines. The CO evaporation radius can be constrained in the empirical models if the temperature structure is well known through dust continuum radiative calculation. The CO evaporation temperature depends on the surface properties of dust grains. For example, if the grain surfaces are covered dominantly by water, then the evaporation temperature should be higher than in the case of the CO-dominant grain surfaces. In addition, if the inside-out collapse model is the correct theory for isolated star formation, the simple models can constrain the infall radius in a star forming core.  $r_{out}$  might be also constrained with the empirical models if the line ratios of appropriate molecules are used.

In this comparison, we should not exclude the possibility that the discrepancy between the empirical model and the full evolutionary model may be a signal that something is missing or incorrect in the chemical description of a specific species, such as an incorrect binding energy, missing reaction, and so on. For example, we did not include surface chemistry, which might be very important in the chemistry of H<sub>2</sub>CO. Schöier et al. (2004) found that a drop abundance profile fitted well the the ratios of many lines and the interferometer data of H<sub>2</sub>CO toward L1448-C and IRAS 16293-2422. In contrast, Evans et al. (2005) showed that neither the evolutionary chemical model nor any step model matched high J lines of H<sub>2</sub>CO in B335.

We tested two static models; one is the truly static model in which physical conditions do not vary with

time, and the other is the partly static model that includes the evolution of physical conditions, but does not consider the dynamical effect in the chemistry. Although the partly static model is much closer to the evolutionary model than the truly static models that previous studies have used, the comparison between the evolutionary model and the partly static model shows that the static models have different profiles than the evolutionary ones, with the differences becoming more apparent at high resolutions and for high energy transitions. As mentioned in previous sections, the difference between the evolutionary model and the static model will be dependent on the velocity structure of a star forming core. Therefore, we have to use high resolution and high-excitation lines to constrain the velocity structure coupled with the abundance profiles. Such constraints are necessary to decide

which theoretical model best explains the star forming process. These observations will be practicable with the CARMA and ALMA in the near future.

We thank E. van Dishoeck for suggesting these comparisons and helpful comments. We also thank J. Jørgensen for useful discussions. This work was supported in part by NSF grant AST-0307250 to the University of Texas at Austin and AST-0335207 to the University of Michigan. Jeong-Eun Lee is grateful to the Department of Astronomy and the University of Texas at Austin for their support through the David Allen Benfield Memorial Scholarship and the University of Texas at Austin Continuing Fellowship.

#### REFERENCES

Ciolek, G.E. & Mouschovias, T.C., 1994, *ApJ*, 425, 142  
 Doty, S.D., van Dishoeck, E.F., van der Tak, F.F.S., & Boonman, A.M.S. 2002, *A&A*, 389, 446  
 Doty, S.D., Schöier, F.L., & van Dishoeck, E.F. 2004, *A&A*, 418, 1021  
 Evans, N.J.,II, Lee, J.-E., Rawlings, J.M.C., & Choi, M. 2005, *ApJ*, in press (astro-ph/0503459)  
 Foster, P.N., & Chevalier, R.A., 1993, *ApJ*, 416, 303  
 Jørgensen, J.K., Schöier, F.L., van Dishoeck, E.F. 2002, *A&A*, 389, 908  
 Jørgensen, J.K., Schöier, F.L., van Dishoeck, E.F. 2004, *A&A*, 416, 603  
 Jørgensen, J.K., Schöier, F.L., van Dishoeck, E.F. 2005, *A&A*, in press  
 Larson, R.B., 1969, *MNRAS*, 145, 271  
 Lee, J.-E., Evans, N.J.,II, Shirley, Y.L., & Tatematsu, K. 2003, *ApJ*, 583, 789  
 Lee, J.-E., Bergin, E.A., & Evans, N.J.II 2004, *ApJ*, 617, 360  
 McLaughlin, D.E., & Pudritz, R.E., 1997, *ApJ*, 476, 750  
 Penston, M.V., 1969, *MNRAS*, 144, 425  
 Schöier, F.L., Jørgensen, J.K., van Dishoeck, E.F., Blake, G.A. 2002, *A&A*, 390, 1001  
 Schöier, F.L., Jørgensen, J.K., van Dishoeck, E.F., Blake, G.A. 2004, *A&A*, 418, 185  
 Shu, F.H. 1977, *ApJ*, 214, 488  
 Shu, F.H., Adams, F. C., & Lizano, S. 1987, *ARA&A*, 25, 23  
 Terebey, S., Shu, F.H., & Cassen, P. 1984, *ApJ*, 286, 529  
 Young, K.E., Lee, J.-E., Evans, N.J.,II, & Goldsmith, P.F. 2004, *ApJ*, 614, 252

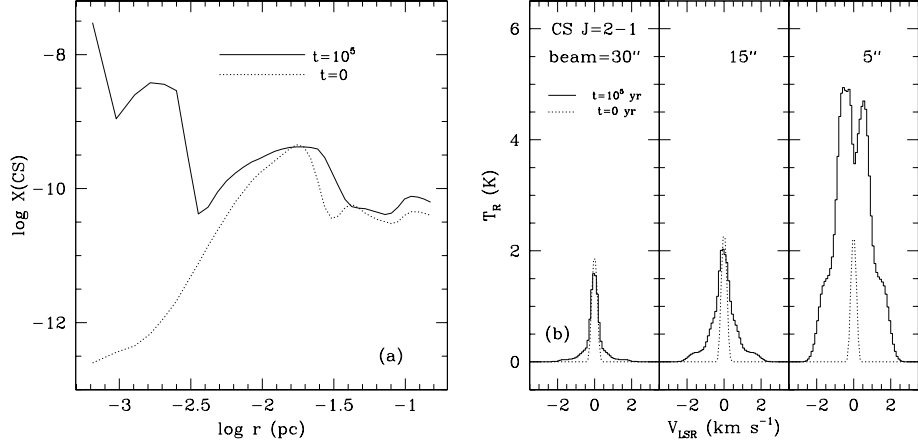


FIG. 1.— Comparison of the CS 2–1 lines from the evolutionary model at  $t = 0$  and  $t = 10^5$  yr; (a) the comparison of abundance profiles at two time steps (solid line for  $t = 10^5$  and dotted line for  $t = 0$ ) and (b) comparison of the CS 2–1 line profiles calculated from the evolutionary model at  $t = 0$  (dotted line) and  $t = 10^5$  (solid line). The evolutionary stages can be distinguished better at higher resolution.

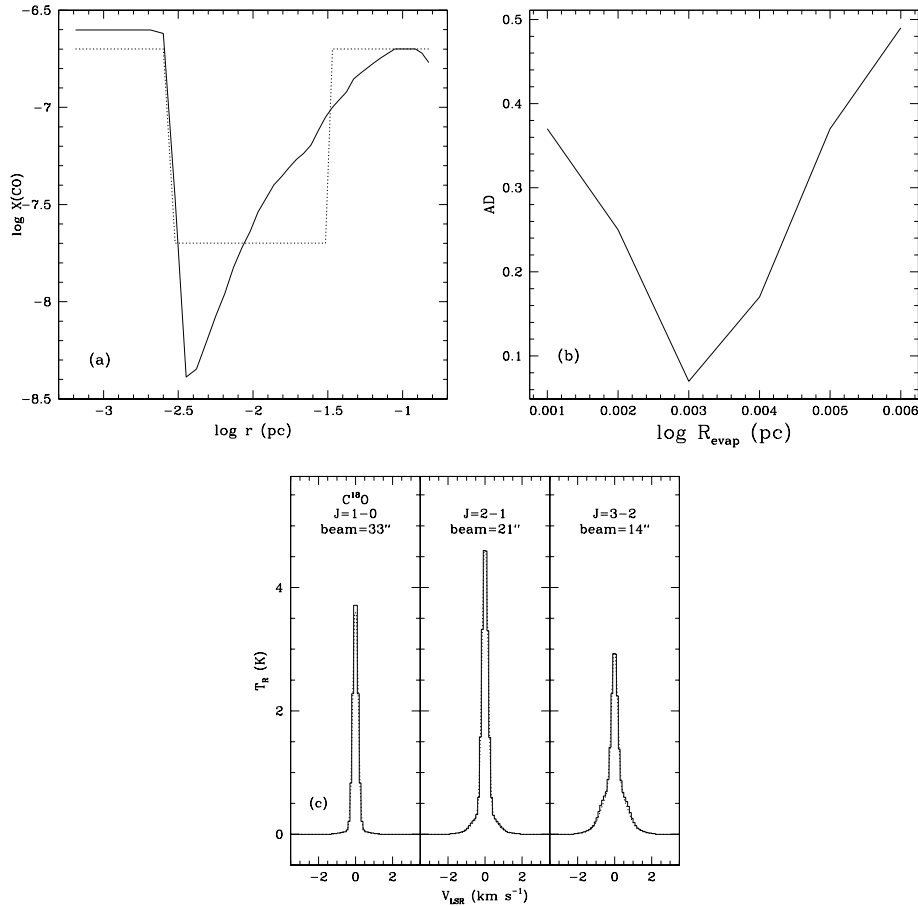


FIG. 2.— Comparison between the evolutionary model at  $t = 10^5$  yr and a drop model in  $\text{C}^{18}\text{O}$ ; (a) the comparison of abundance profiles in two models (solid line for the evolutionary model and dotted line for the best-fit drop model to the evolutionary model), (b) the absolute deviation of integrated intensities vs. the evaporation radius in the drop model, which is calculated over three  $\text{C}^{18}\text{O}$  line profiles simulated with two abundance models, and (c) the comparison of the  $\text{C}^{18}\text{O}$  line profiles of the evolutionary model (solid line) and the best-fit drop model (dotted line) to the evolutionary model in three different transitions.

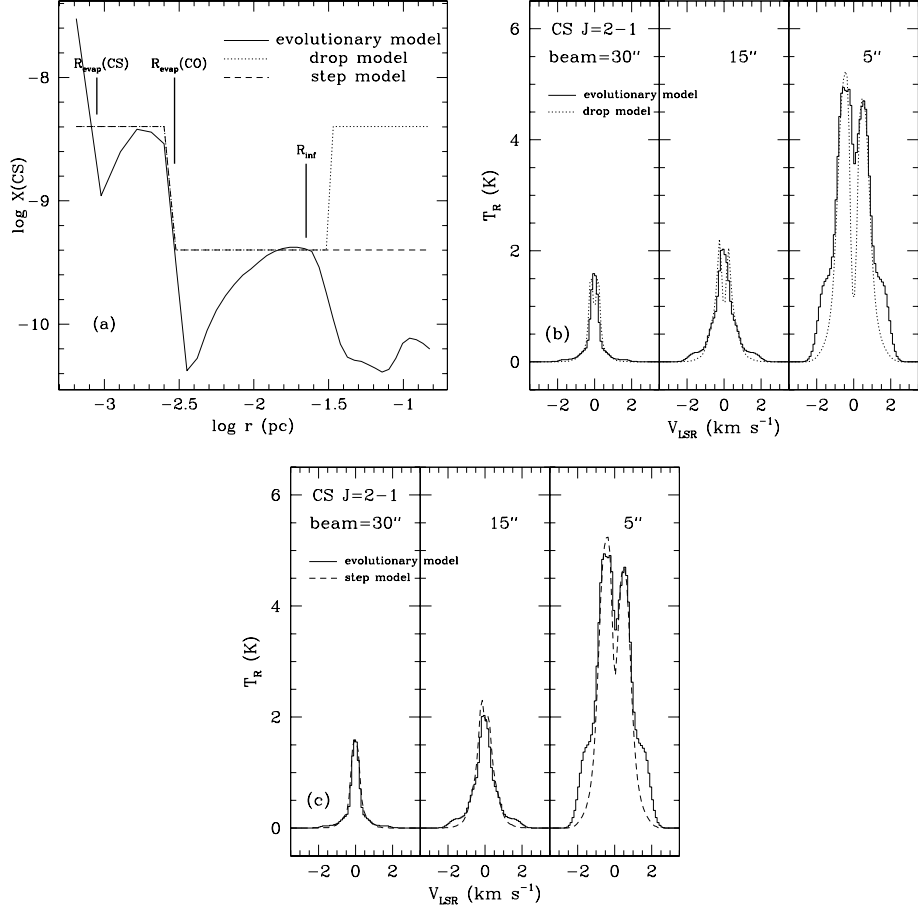


FIG. 3.— Comparison between the evolutionary model at  $t = 10^5$  yr, a drop model, and a step model in CS; (a) the comparison of abundance profiles in three models (solid line for the evolutionary model and dotted and dashed lines for the best-fit drop and step models to the evolutionary model, respectively), (b) the comparison of the CS 2–1 line profiles of the evolutionary model (solid line) and the best-fit drop model (dotted line) to the evolutionary model with three different resolutions. and (c) the comparison of the CS 2–1 line profiles of the evolutionary model (solid line) and the best-fit step model (dashed line) to the evolutionary model with three different resolutions. In (a), thick vertical lines indicate the evaporation radii of CS and CO.

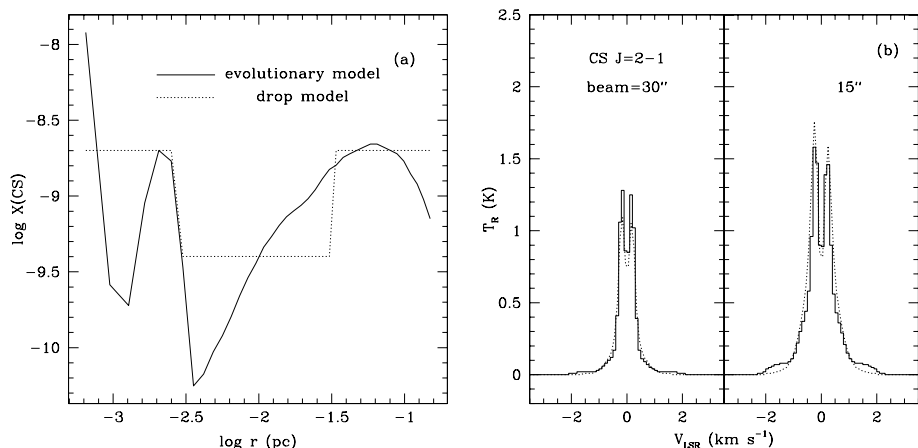


FIG. 4.— Comparison between the evolutionary model with an external extinction of 3 mag at  $t = 10^5$  yr and a drop model in CS; (a) the comparison of abundance profiles in two models (solid line for the evolutionary model with 3 mag of external extinction and dotted line for the best-fit drop model to the evolutionary model) and (b) comparison of the CS line profiles calculated from the evolutionary model with an external extinction of 3 mag (solid line) and the best-fit drop model (dotted line) to the evolutionary model with two different resolutions.

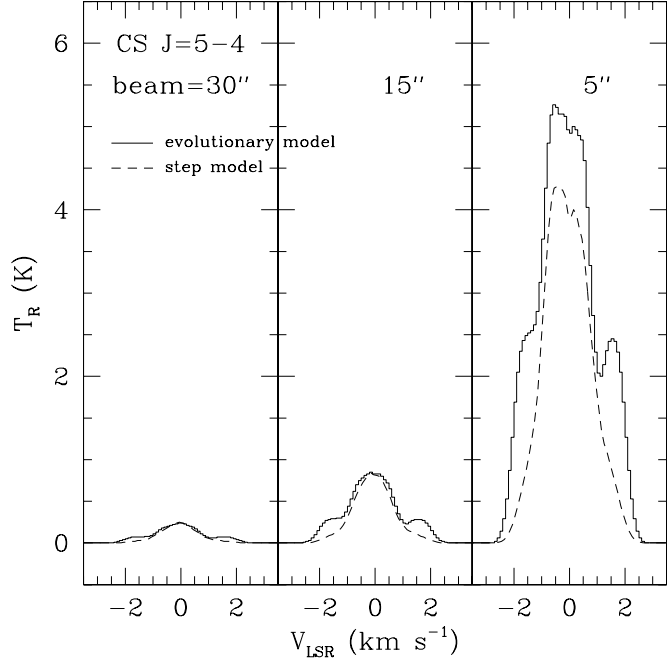


FIG. 5.— The comparison of the CS 5–4 line profiles simulated with the abundance profiles of the evolutionary model (solid line) and the step model (dashed line) in Fig. 3a.

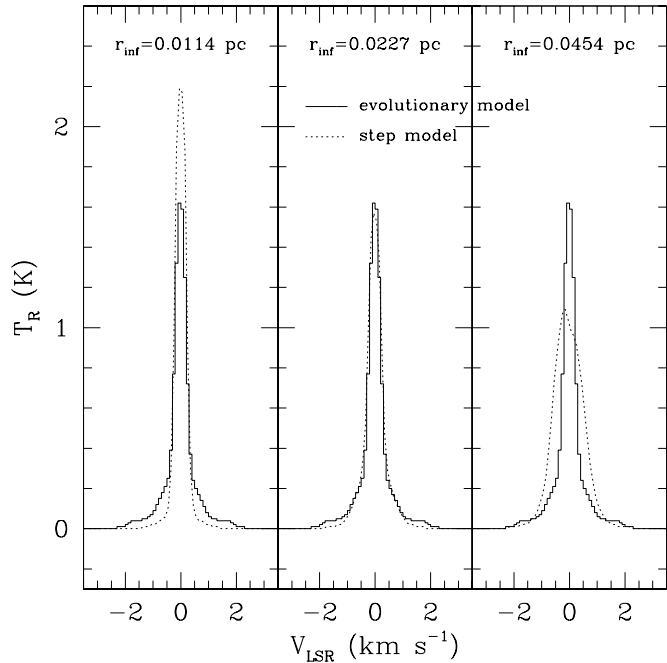


FIG. 6.— The CS 2–1 line profile (solid line) simulated from the evolutionary model at  $t = 10^5$  yr is compared with profiles (dotted line) predicted by step models with different infall radii. The beam size for this test is  $30''$ . The first panel shows the best model with  $r_{inf} = 0.0114$  pc; the second panel shows the best model with  $r_{inf} = 0.0227$  pc, which is the infall radius at  $t = 10^5$  yr; the third panel shows the best model with  $r_{inf} = 0.0454$  pc. The second panel shows the same comparison as the first panel in Fig. 3c does.

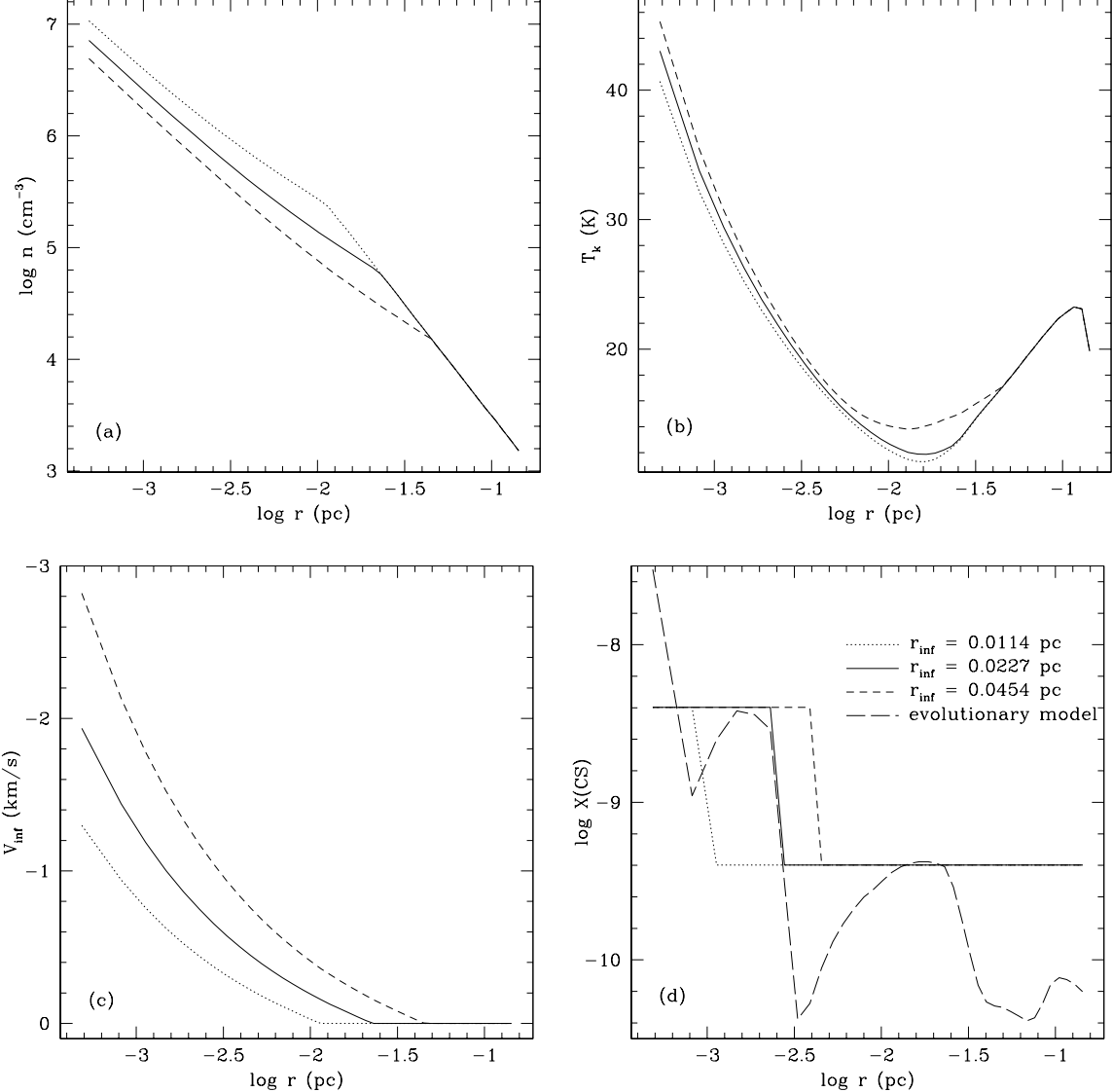


FIG. 7.— Physical properties used for testing different infall radii with the step models in abundance; (a) density, (b) kinetic temperature, (c) velocity, and (d) abundance structure for the three infall radii: 0.0114 (dotted line), 0.0227 (solid), and 0.0454 (dashed) pc. In the abundance structures, the long dashed line represents the one from the evolutionary model, which is considered as a standard model in this test.

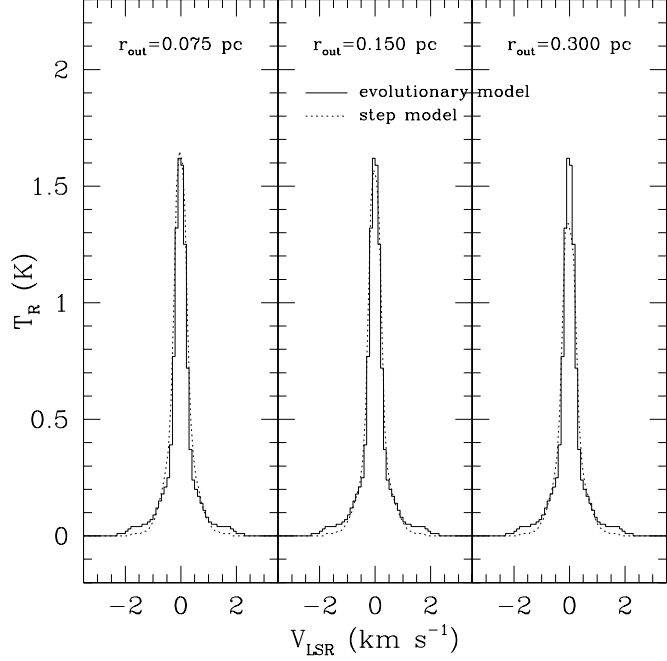


FIG. 8.— The CS 2–1 line profile (solid line) simulated from the evolutionary model at  $t = 10^5$  yr is compared with profiles (dotted line) predicted by the step model with different outer radii but the same infall radius of 0.0227 pc. The kinetic temperature structure for each model has been calculated self-consistently. The beam size for this test is  $30''$ . The step abundance structure used in this test is the same as the one (dashed line) in Fig. 3a. The first panel shows the model with  $r_{out} = 0.075$  pc; the second panel shows the model with  $r_{out} = 0.150$  pc, which is the standard outer radius for this work; the third panel shows the model with  $r_{inf} = 0.300$  pc. The second panel shows the same comparison as the first panel in Fig. 3c does.

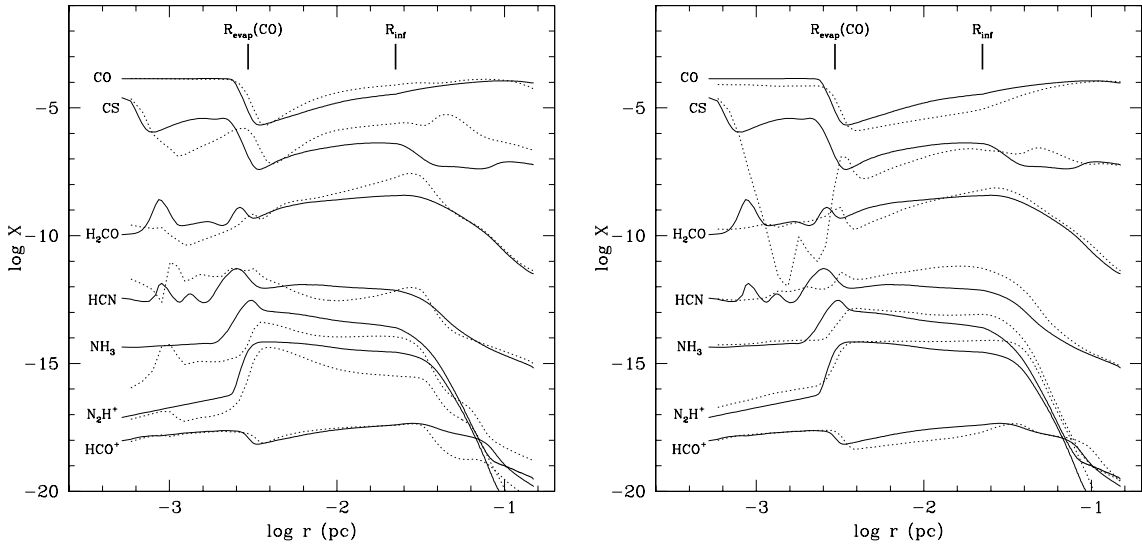


FIG. 9.— The comparisons of abundance profiles calculated by the evolutionary model (solid lines) at  $t = 10^5$  yr with the truly static model (dotted line) at  $t = 10^5$  yr (left box) and  $t = 1.1 \times 10^6$  yr (right box). The infall radius and the evaporation front of CO are around 0.023 and 0.003 pc, respectively, and marked with thick vertical lines. Profiles have been shifted up and down for better comparison. CS is shifted up by 3.0 orders of magnitude, and  $H_2CO$ ,  $HCN$ ,  $NH_3$ ,  $N_2H^+$ , and  $HCO^+$  are shifted down by 0.5, 3.5, 6.0, 5.5, and 9.0 orders of magnitude, respectively.

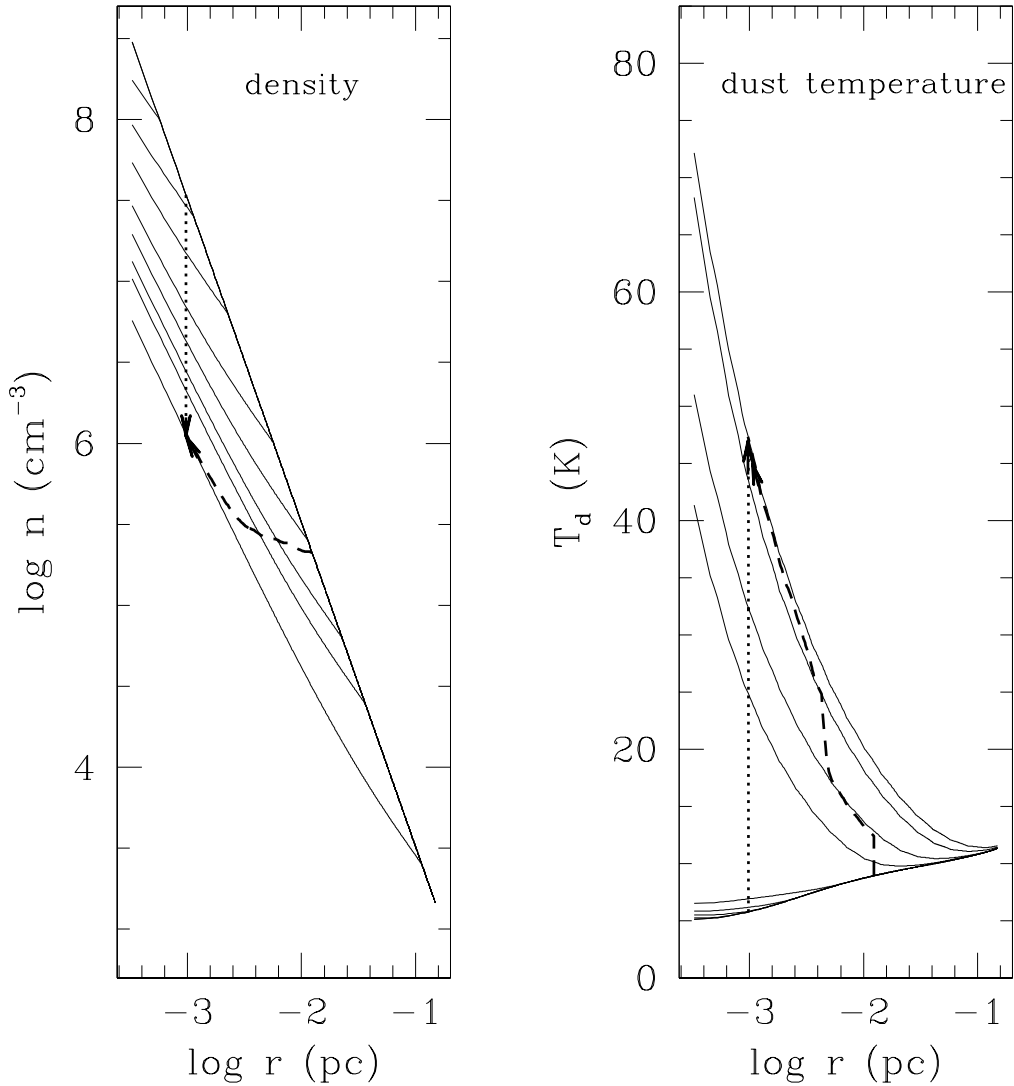


FIG. 10.— Two different evolutionary histories of density and temperature in the static model and the evolutionary model. The solid lines represent the density (left box) and temperature (right box) structures at the time steps of 0,  $2.5 \times 10^3$ ,  $5^3$ ,  $10^4$ ,  $2.5 \times 10^4$ ,  $5 \times 10^4$ ,  $10^5$ ,  $1.6 \times 10^5$ , and  $5 \times 10^5$  yr. The dotted and dashed lines indicate the routes along which the static and evolutionary models, respectively, calculate the chemical evolution. In the static model, the chemical evolution is calculated at a given radius, so density decreases with time (from top to bottom), but temperature increases with time (from bottom to top). However, in the evolutionary model, the chemical evolution is calculated following a gas parcel, which falls toward the center (from right to left). Consequently, both density and temperature increase with time.

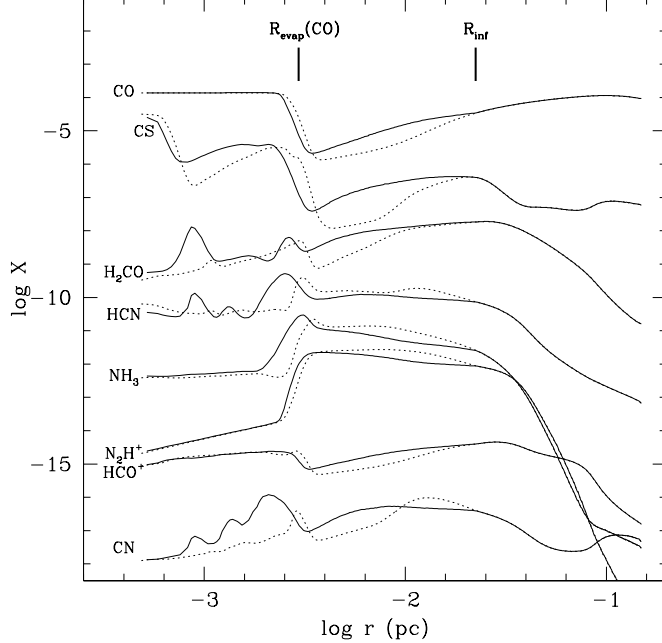


FIG. 11.— The comparison of abundance profiles calculated by the evolutionary model (solid lines) and the static model (dotted lines) at  $t = 10^5$  yr. The infall radius and the evaporation front of CO are around 0.023 and 0.003 pc, respectively. Profiles have been shifted up and down for better comparison. CS, H<sub>2</sub>CO are shifted up by 3.0 and 0.2 orders of magnitude, and HCN, NH<sub>3</sub>, N<sub>2</sub>H<sup>+</sup>, HCO<sup>+</sup>, and CN shifted down by 1.5, 4.0, 3.0, 6.0, and 8.0 orders of magnitude, respectively.

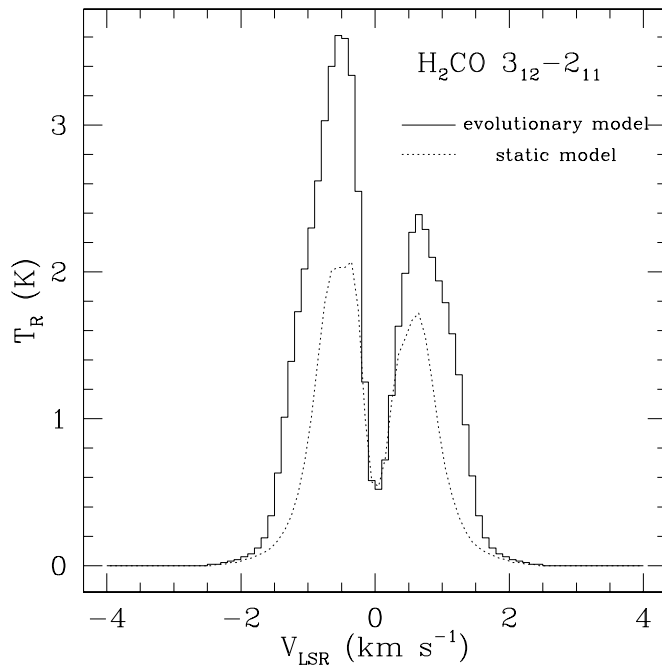


FIG. 12.— The comparison of the ortho-H<sub>2</sub>CO line profiles resulting from the evolutionary model (solid line) and the static model (dotted line) at  $t = 10^5$  yr. The abundance profiles used for the line profiles are plotted in Fig. 11. The spatial resolution is 3''.